Surface-Enhanced Raman Signal for Terbium Single-Molecule Magnets Grafted on Graphene

Manuel Lopes,[†] Andrea Candini,[†,‡] Matias Urdampilleta,[†] Antoine Reserbat-Plantey,[†] Valerio Bellini,[‡] Svetlana Klyatskaya,[§] Laëtitia Marty,[†] Mario Ruben,[§,⊥] Marco Affronte,[∥,¶] Wolfgang Wernsdorfer,[†] and Nedjma Bendiab[†,*]

[†]Institut Néel, associé à l'Université Joseph Fourier, CNRS, BP 166, 38042 Grenoble Cedex 9, France, [‡]CNR-Institute of NanoSciences S3 via Campi 213/a, 41125 Modena, Italy, [§]Institute of Nanotechnology, Karlsruhe Institute of Technology (KIT), 76344 Eggenstein-Leopoldshafen, Germany, [⊥]IPCMSCNRS-Université de Strasbourg, 67034 Strasbourg, France, [∥]CNR-Institute of NanoSciences S3 via Campi 213/a, 41100 Modena, Italy, and [¶]Dipartimento di Fisica, Università di Modena e Reggio Emilia, via Campi 213/a, 41125 Modena, Italy

ABSTRACT We report the preparation and characterization of monolayer graphene decorated with functionalized single-molecule magnets (SMMs). The grafting ligands provide a homogeneous and selective deposition on graphene. The grafting is characterized by combined Raman microspectroscopy, atomic force microscopy (AFM), and electron transport measurements. We observe a surface-enhanced Raman signal that allowed us to study the grafting down to the limit of a few isolated molecules. The weak interaction through charge transfer is in agreement with *ab initio* DFT calculations. Our results indicate that both molecules and graphene are essentially intact and the interaction is driven by van der Waals forces.

KEYWORDS: graphene · Raman spectroscopy · bis(phthalocyaninato)terbium(III) · single-molecule magnets · AFM · $\pi-\pi$ interaction

Graphene has been attracting considerable interest due to its fascinating electrical and mechanical properties. High crystalline order,[1] ballistic transport, massless Dirac fermion-like charge carriers,[2] as well as long spin coherence length due to the intrinsically low spin−orbit coupling make graphene a promising candidate for applications in electronics,[3] spintronics,[4] and nanomechanics.[5] Along this line, field-effect transistors (FETs)[6] and graphene−SQUID devices[7] have been demonstrated. The fact that graphene is a one-atom-thick layer directly exposed to the external world makes it a promising material for ultrasensitive probes and opens the possibility to exploit proximity effects and chemical functionalization. For instance, graphene-based gas detectors with a sensitivity down to the single-molecule limit have been demonstrated.[8] Graphene−metal interface or molecular functionalization has been reported to induce superconductivity,[9,10] insulating behavior,[11] or magnetic properties.[12,13]

In the past few years, we have started developing hybrid nanoarchitectures combining carbon-based structures and single-molecule magnets (SMM)[14−17] in view of molecular spintronic devices.[18] SMMs are metal-ion complexes exhibiting quantum phenomena at low temperatures.[19,20] They might be suitable as components for quantum computing[21,22] and molecular spintronics.[18,23]

The objective of this study is to graft in a controlled way SMMs on graphene-based devices using functional ligands equipped with appropriate linkers and to investigate the interaction between graphene and SMMs. While covalent bonding might severely alter the performance of the devices by a strong lifting of graphene sp^2 character, noncovalent π-stacking should preserve the intrinsic features of both graphene and SMMs and lead to an indirect coupling through, for instance, the SMM magnetic stray field. Among the large variety of SMMs, mononuclear representatives like the rare-earth-based bis(phthalocyaninato) complexes (so-called double deckers) are particularly attractive.[15] Their robust monatomic structure opens the possibility for chemical tuning of the molecular properties, while maintaining the overall coordinating core and therefore their SMM behavior. Herein, a bis(phthalocyaninato)terbium(III) complex particularly tailored for the grafting on sp^2 carbon surfaces was used (Figure 1a and Experimental Section).[15]

Combining AFM and Raman investigations, we show here the selective and homogeneous grafting of SMMs on

*Address correspondence to nedjma.bendiab@grenoble.cnrs.fr.

Received for review July 30, 2010 and accepted November 02, 2010.

Published online November 10, 2010. 10.1021/nn1018363

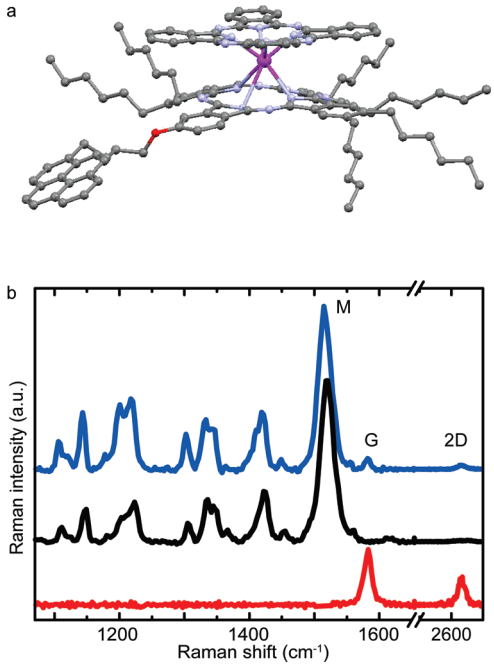

Figure 1. (a) Scheme of $TbPc_2$ molecule constituted by a single magnetic Tb^{3+} ion coordinated by two phthalocyanine ligands. One of the ligands is subtituted by a pyrene group and six hexyl groups. (b) Raman spectra of the pristine graphene (bottom, red), $TbPc_2$ powder (middle, black), and the hybrid system graphene and $TbPc_2$ molecules (top, blue). The G and 2D modes of graphene and the M band of $TbPc_2$ molecules are indicated.

graphene and the structural integrity of the molecule after the grafting. With respect to the techniques traditionally employed to study molecules on surfaces (AFM, STM), Raman spectroscopy can probe structural and electronic properties of both molecules and graphene in a fast and nondestructive way.[24,25] The enhanced Raman intensity signal of these SMMs on graphene allowed studies down to few isolated molecules on the surface. The weak orbital overlapping between graphene and SMM suggested by our experiments is corroborated by *ab initio* calculations and electron transport measurements.

RESULTS AND DISCUSSION

Figure 1b presents typical Raman spectra of pristine graphene, $TbPc_2$ powder, and the graphene−$TbPc_2$ hybrid. Note that Raman scattering is resonant when the excitation energy matches an electronic transition of $TbPc_2$,[15] which is the case at the excitation wavelength used here. The Raman response of the graphene−$TbPc_2$ hybrid is a simple superposition of the response of each component without any shift or disappearance of a mode, indicating that both remain chemically unchanged after the grafting process. The spectrum obtained on $TbPc_2$ powders shows several peaks between 1050 and1650 cm^{-1}. In particular, the M mode in Figure 1b is a doublet with 1512 and 1520 cm^{-1}, which was ascribed to the pyrrole C═C and aza-C═N stretching modes, respectively. It was found that these frequencies depend on the ionic radius of the rare-earth complexes.[26,27] Since all Raman modes of the $TbPc_2$ molecule followed the same behavior in our experiments, the most intense band (M) was used for the Raman maps. As presented in Figure 2a, the spatially resolved Raman map of $TbPc_2$ molecules precisely matches the graphene G band map (Figure 2b), while no $TbPc_2$ Raman signal is detectable on the silicon substrate.

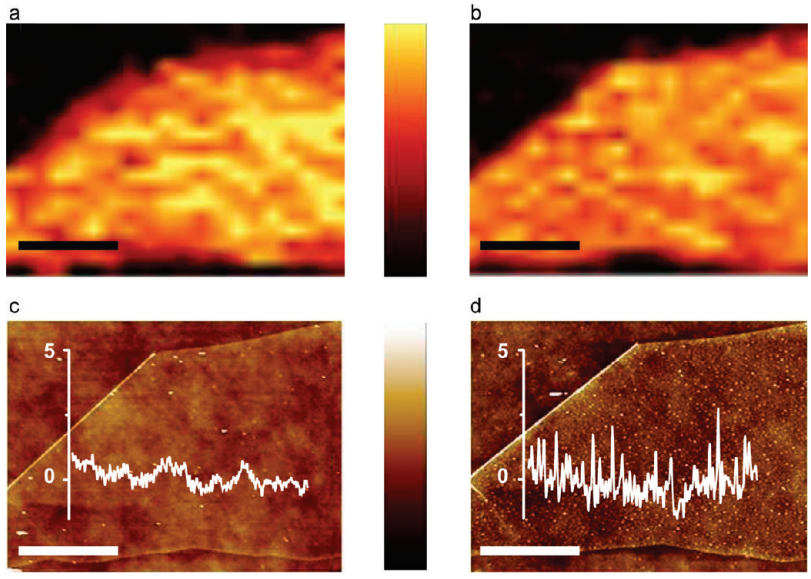

Figure 2. (a,b) Spatially resolved Raman intensity map of the $TbPc_2$ M band and of the graphene G band, respectively. Color scale range: 0 to 200 CCD counts from black to yellow. (c,d) AFM topography image and height profile of the pristine graphene of the graphene−$TbPc_2$ hybrid system, respectively. Color scale range: 0 to 10 nm from black to white. For panels a, b, and d, the sample was prepared with a solution concentration of 10^{-8} mol · L^{-1} (scale bars = 3 μm).

AFM measurements confirm this result because the roughness on the graphene after grafting is much more pronounced than before grafting, whereas the roughness hardly changed on the silicon oxide (Figure 2d). The 2−3 nm high roughness is associated with the formation of molecular clusters of few molecules (<5) packed together. For concentrations higher than 10^{-5} mol · L^{-1}, the AFM topography reveals the presence of much large clusters (up to 10−20 nm in size), which are uniformly distributed without any evidence for grafting selectivity. Indeed, molecular clusters also appear on silicon oxide, as confirmed by a weak $TbPc_2$ Raman signal (see Supporting Information). These observations establish that the grafting mechanism is selective and favors deposition on graphene, which is important for hybrid device fabrication. Moreover, all $TbPc_2$ Raman modes are present on the Raman spectrum of the hybrid with the same frequency position and width as for the $TbPc_2$ powder (Figure 1b).

In particular, no extra peak was observed. The G band of graphene is only slightly shifted and without any broadening or splitting.[28] These observations point to a weak interaction between $TbPc_2$ and graphene.

In order to get more insight, contact mode AFM was used to selectively displace the molecules grafted on graphene (Figure 3a). After performing contact AFM, the graphene surface recovered a small roughness and was free of visible clusters, as shown in Figure 3a, suggesting that the majority of all $TbPc_2$ molecules were displaced by the tip. From the AFM profile shown in Figure 3c, we estimate the volume corresponding to the displaced molecules; we found that the values measured on graphene flakes are at least factor of 10 larger than what we found on the SiO_2 surface. Along with AFM measurements, we recorded Raman maps on the same cleaned area (Figure 3b). The $TbPc_2$ Raman signal strongly decreases in the cleaned area, although a weak residual signal (about 15%) is still detected in the center of the scan (red curve in Figure 3e), suggesting that a small amount of molecules is left on the cleaned graphene. In particular, while AFM measurements indicate that an important quantity of molecules is present on the edges (Figure 3b), the corresponding Raman signal is increased only by a factor of 1.4 with respect to the decorated graphene (Figure 3d,e). We can, therefore, conclude that the $TbPc_2$ Raman signal does not change linearly with the quantity of deposited molecules. Additional evidence of the Raman enhancement is provided by Raman measurements for successive deposition of different $TbPc_2$ concentrations. Figure 4a,b displays the dependence of the $TbPc_2$ doublet Raman intensity on different concentrations up to 10^{-6} mol · L^{-1}. The intensity follows a logarithmic behavior which saturates at 10^{-7} mol · L^{-1}. This nonlinear Raman response is compatible with a chemical enhancement due to a modification of the molecule polarizability, as recently proposed by Ling *et al.*,[29] *via* a charge transfer with the substrate.[30−32] This effect occurs only for molecules in contact with graphene,[30] and therefore, only the first molecular monolayer is influenced, in agreement with the observed signal saturation for thicker molecular films. Furthermore, the graphene-induced chemical enhancement allows the detection of the SMMs' Raman signal for concentrations as low as 10^{-10} mol · L^{-1} (Figure 4c), while no significant roughness

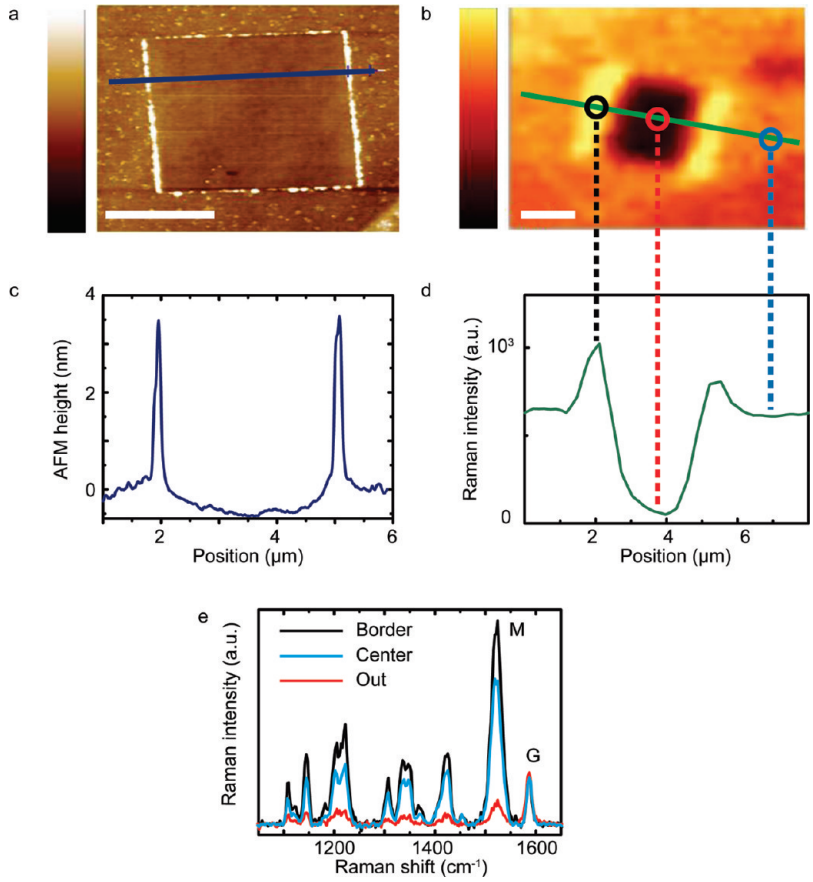

Figure 3. (a) Tapping AFM topography image performed after contact AFM cleaning on a 2 μm × 2 μm square to displace the $TbPc_2$ single-molecule magnet on the graphene. Color scale range: 0 to 10 nm from black to white. (b) Raman intensity map of the $TbPc_2$ M band for the same place as in panel a. Color scale range: 0 to 200 CCD counts from black to yellow. (c) Height profile of the graphene surface along the blue line represented in panel a. (d) Raman intensity profile along the green curve shown in panel b. (e) Raman spectra taken at three different spots indicated by the colored circles in panel b: center (red), border (black), and outside (blue) (scale bars = 1 μm).

change was detected on graphene by AFM. We suggest that, at low concentrations, the few deposited molecules detected by the Raman signal are isolated on the graphene surface and difficult to extract from the AFM background signal. In conclusion, the $TbPc_2$−graphene interaction improves the Raman detection limit, which is estimated below 100 molecules under the laser spot of 500 nm.[33] This sensitivity is remarkable and leads us to conclude that within this level of accuracy no particular change of the molecular structural and electronic features was observed. Despite the described strong impact on the Raman response, the molecule−graphene interaction seems to be weak.

In order to elucidate this experimental findings, *ab initio* density functional theory calculations were performed. To keep the problem tractable from the computational point of view, we studied the anchoring properties of the pyrene group alone (Figure 4e,f). Recent combined scanning probe and XMCD work has shown that unsubstituted $TbPc_2$ molecules adsorb flat lying on both copper[33] and graphite[34] surfaces with the

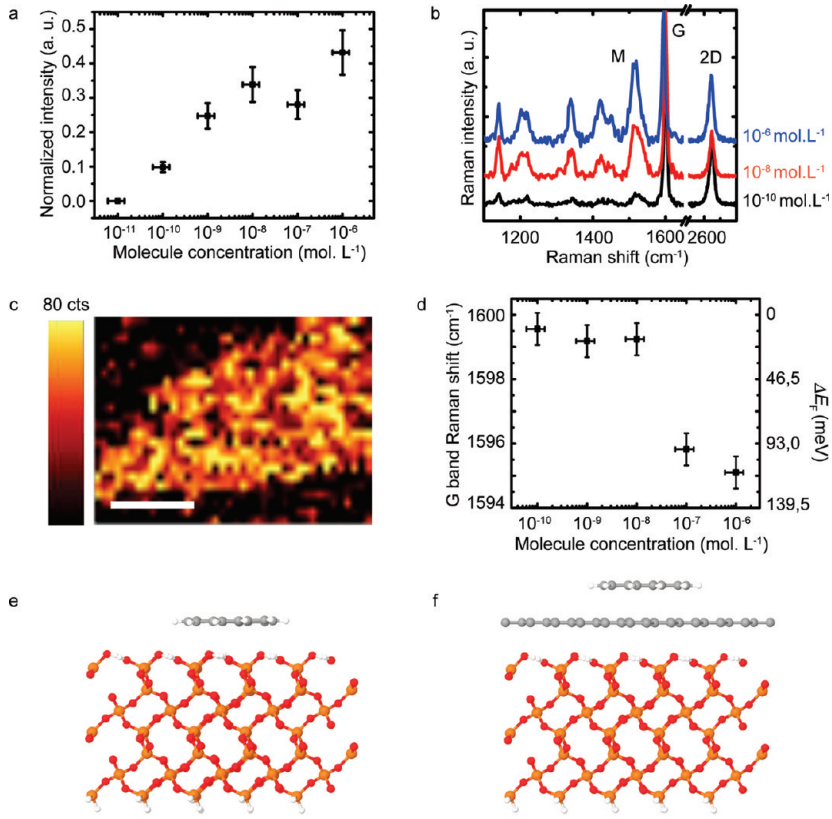

Figure 4. (a) Evolution of the M doublet intensity according to the solution concentration. (b) Raman spectra of $TbPc_2$ molecules deposited on graphene at three different concentrations. (c) Raman intensity map of the $TbPc_2$ deposited with a concentration of 10^{-10} mol · L^{-1}. (d) Evolution of the position of the graphene G band with $TbPc_2$ concentration. The value for the pristine system was 1600 cm^{-1}. (e) Pyrene molecule anchored to clean SiO_2 surface. (f) Pyrene molecule anchored to graphene on SiO_2 (scale bar = 3 μm).

magnetic anisotropy axis orthogonal to the surface normal.[35] Due to the chemical composition of the phthalocyanine (Pc) groups in $TbPc_2$, characterized also by π-delocalized orbitals, it is possible to assume that Pc and pyrene groups interact similarly with the underlying substrate. In Figure 4e,f, we present a sketch of the two systems that we have considered, namely, a pyrene molecule adsorbed on a clean and graphene-covered SiO_2 surface (Figure 4e,f). More details on the method and the simulated systems are given in the Supporting Information. We find that the interaction between pyrene and graphene (or SiO_2) is noncovalent and due to van der Waals interactions. This leads to an equilibrium distance of 3.2 and 2.8 Å between pyrene and graphene or SiO_2, respectively. Most importantly, our calculations indicate that a pyrene group adsorbs more favorably on the graphene layer than on the SiO_2 surface, in agreement with the experimental evidence discussed above. The binding energy of the pyrene molecule on graphene is indeed 2-fold larger than that for the pyrene adsorbed directly on SiO_2: ΔE(Py + graphene + SiO_2) = 1.06 eV *vs* ΔE(Py + SiO_2) = 0.52 eV. Finally, the orbital overlapping, although weak, still induces changes in the electronic properties of the graphene. In Figure 4d, we plot the G band frequency dependence on the $TbPc_2$ concentration. Indeed, the G band is slightly shifted to lower frequency (4 cm^{-1} between extreme concentrations) as well as the 2D band (3 cm^{-1} between extreme concentrations). This frequency shift is compatible with a doping-induced change of the Fermi energy.[25,36] The corresponding relative change of the Fermi energy of graphene (reported on the right axis of Figure 4d) is calculated from our Raman shift, following the work of Yan *et al.*[25] and Pisana *et al.*[37] The observed logarithmic decay suggests that the doping originates only from the molecules in contact with graphene. Although it is strongly dependent on the intrinsic doping of the pristine layer and undetectable for multilayer flakes, this frequency shift is reproducible for any monolayer at the highest molecular concentration with a typical charge transfer of 10^{12} e/cm^2. Though predicted by *ab initio* calculations, these data obtained on a nonconnected graphene monolayer need to be confirmed by measuring the electronic properties of a monolayer with a well-defined electrical potential, as presented in the following. In order to further probe the consequences of grafting on the electronic properties, we performed electron transport measurements under ambient conditions on a similar graphene flake in a FET geometry (inset of Figure 5b). For increasing $TbPc_2$ concentrations, the Dirac point (corresponding to the minimum of conductance) shifts

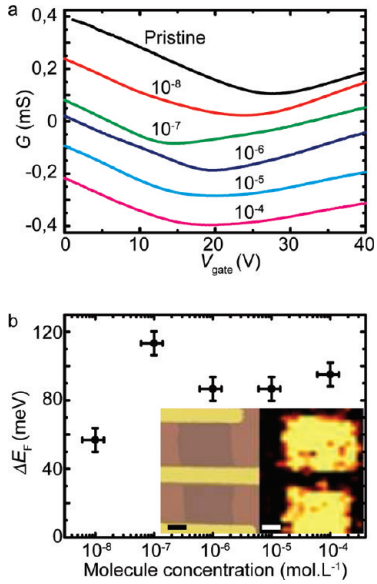

Figure 5. (a) Transfer characteristics (I, V_g) of the graphene FET for different $TbPc_2$ concentrations. The measurements have been performed under ambient conditions using the lock-in technique with an AC excitation of 100 μV. Curves are vertically shifted (by −0.3 mS) for clarity. (b) Concentration dependence of the shift of the Fermi energy relative to the pristine device. Inset: optical image and Raman intensity map of the M doublet of the device (scale bars = 1 μm).

toward lower gate voltages, which suggests an electron transfer from the $TbPc_2$ molecules to the graphene, that is, n-doping (Figure 5a). Despite a slight asymmetry between electrons and holes induced by molecule decoration, the graphene mobility $\mu = \sigma/ne$ (where n is the density of carriers[38] and e the electron charge) remains constant at ≈2000 $cm^2 \cdot V^{-1} \cdot s^{-1}$ until the concentration reaches about 10^{-6} $mol \cdot L^{-1}$. This indicates that no significant disorder is induced in the graphene. For concentrations higher than 10^{-5} $mol \cdot L^{-1}$, the mobility drops by nearly 40% and the conductivity minimum broadens significantly. This is consistent with the presence of clusters and crystallites at these high concentrations, which induce defects and diffusion sites on the graphene sheet and degrade progressively the mobility. The relative change of the Fermi energy caused by the $TbPc_2$ molecules is calculated from the electrical transport measurements and reported on Figure 5b. The logarithmic behavior and the shift magnitude are in good agreement with the values obtained from the Raman frequency shift. Finally, Raman and transport experiments converge on a charge transfer between graphene and molecules of about 10^{12} e/cm^2 that corresponds to 10^{-4} electrons per carbon atom for the highest concentration (10^{-4} $mol \cdot L^{-1}$), indicating that the electronic properties of graphene and $TbPc_2$ are not altered.

CONCLUSION

We report herein evidence for a selective physisorption and homogeneous grafting of pyrene-substituted $TbPc_2$ single-molecule magnets onto graphene. The decoration process is directly applicable *in situ* onto graphene transistors. The enhanced Raman intensity of $TbPc_2$ on graphene allows the detection of molecules down to a few tens of molecules per laser spot. Furthermore, a weak electronic interaction between graphene and $TbPc_2$ molecules was found. Only small charge transfer occurs, resulting in a shift of Fermi level and preserving graphene mobility. Our experimental findings are corroborated by DFT calculations that point out van der Waals coupling between pyrene and graphene, leading us to conclude that $TbPc_2$ and graphene electronic properties are essentially intact even for low molecule densities where no molecular clusters are observed. Note that our main results can be applied to other families of molecular systems with different functionalities since a similar pyrene substitution can be performed on many other compounds. Our results show a way to probe the interactions and to provide fabrication criteria in carbon-based molecular sensors for spintronics applications.

EXPERIMENTAL SECTION

We deposited graphene flakes by micromechanical exfoliation[39] of natural graphite on degenerately doped Si with a 300 nm SiO_2 capping layer. Optical microscopy and AFM were used to determine the flake thickness and position, and the number of layers was also confirmed by Raman spectroscopy (up to 5 layers).[40] For FET devices, e-beam lithography was performed by alignment on prelocated graphene flakes. Ten nanometer Ti/100 nm Pt contacts were deposited by electron-gun evaporation on top of the graphene. The silicon substrate was used as a backgate. The SMMs deposited on graphene are pyrenyl-substituted heteroleptical bis(phthalocyaninato)terbium(III) complexes[15] (Figure 1a), referred to as $TbPc_2$ in this publication. This molecule consists of a single magnetic Tb^{3+} ion coordinated to two phthalocyanine ligands (see scheme of Figure 1a). In order to improve the grafting on graphene, one of the two phthalocyanine macrocycles was substituted by a pyrene group and functionalized with six hexyl groups. Both pyrene groups and alkyl chains are well-known to exhibit an attractive interaction with sp^2 carbon materials, maximizing the intermolecular van der Waals interactions.[15,41] The molecule was deposited by drop casting of a $TbPc_2$ solution in dichloromethane (DCM) with a molecule concentration ([$TbPc_2$]) ranging from 10^{-11} to 10^{-4} $mol \cdot L^{-1}$. After 5 s, the sample was rinsed in DCM and dried under nitrogen flow. Residual DCM was removed by a second rinse with isopropanol. The washing efficiency is monitored by a strong decrease of DCM fluorescence, which is a broad band centered at 1600 cm^{-1}. Micro-Raman spectroscopy was performed with a commercial Witec Alpha 500 spectrometer in a backscattering configuration. The excitation wavelength for all presented Raman experiments was the 633 nm line of a He−Ne laser with a power around 300 μW on the sample to prevent any damage of $TbPc_2$ and graphene. All Raman spectra were recorded with a 500 nm diameter laser spot. The spectrometer was equipped with a piezostage, which allows the measurement of Raman intensity maps: a Raman spectrum was recorded for each

pixel (500 nm size), and the integrated intensity of a chosen mode was displayed with a color scale. Tapping and contact mode AFM micrographs were recorded using a VEECO D3100 under ambient conditions.

Acknowledgment. This work has been supported by the ERC advanced grant MolNanoSpin (No. 226558), EU FP7-ICT FET Open "MolSpinQIP" project, Contract N.211284, and the ANR-Pnano project MolNanoSpin. Computational resources have been granted by the project "AMNOS" under the DEISA-Extreme Computing Initiatives. The authors thank V. Reita, E. Eyraud, L. del-Rey, D. Lepoittevin, R. Haettel, and Nanofab facility for technical support.

Supporting Information Available: Additional experimental details and figures. This material is available free of charge *via* the Internet at http://pubs.acs.org.

REFERENCES AND NOTES

1. Geim, A. K.; Novoselov, K. S. The Rise of Graphene. *Nat. Mater.* **2007**, *6*, 183–191.
2. Zhang, Y.; Tan, Y.-W.; Stormer, H. L.; Kim, P. Experimental Observation of the Quantum Hall Effect and Berry's Phase in Graphene. *Nature* **2005**, *438*, 201–204.
3. Neto, A. C.; Guinea, F.; Peres, N.; Novoselov, K.; Geim, A. The Electronic Properties of Graphene. *Rev. Mod. Phys.* **2009**, *81*, 109–162.
4. Tombros, N.; Jozsa, C.; Popinciuc, M.; Jonkman, H.; van Wees, B. Electronic Spin Transport and Spin Precession in Single Graphene Layers at Room Temperature. *Nature* **2007**, *448*, 571–574.
5. Bunch, J.; van der Zande, A.; Verbridge, S.; Frank, I.; Tanenbaum, D.; Parpia, J.; Craighead, H.; McEuen, P. Electromechanical Resonators from Graphene Sheets. *Science* **2007**, *315*, 490–493.
6. Xia, F.; Farmer, D.; ming Lin, Y.; Avouris, P. Graphene Field-Effect Transistors with High On/Off Current Ratio and Large Transport Band Gap at Room Temperature. *Nano Lett.* **2010**, *10*, 715–718.
7. Girit, C.; Bouchiat, V.; Naaman, O.; Zhang, Y.; Crommie, M. F.; Zettl, A.; Siddiqi, I. Tunable Graphene dc Superconducting Quantum Interference Device. *Nano Lett.* **2009**, *9*, 198–199.
8. Schedin, F.; Geim, A.; Morozov, S.; Hill, E.; Blake, P.; Katsnelson, M.; Novoselov, K. Detection of Individual Gas Molecules Adsorbed on Graphene. *Nat. Mater.* **2007**, *6*, 652–655.
9. Kessler, B.; Girit, C.; Zettl, A.; Bouchiat, V. Tunable Superconducting Phase Transition in Metal-Decorated Graphene Sheets. *Phys. Rev. Lett.* **2010**, *104*, 047001.
10. Heersche, H.; Jarillo-Herrero, P.; Oostinga, J.; Vandersypen, L.; Morpurgo, A. Bipolar Super-Currents in Graphene. *Nature* **2006**, *446*, 56–59.
11. Elias, D.; Nair, R.; Mohiuddin, T.; Morozov, S.; Blake, P.; Halsall, M.; Ferrari, A.; Boukhvalov, D.; Katsnelson, M.; Geim, A.; *et al.* Control of Graphene's Properties by Reversible Hydrogenation: Evidence for Graphane. *Science* **2009**, *323*, 610–613.
12. Krasheninnikov, A.; Lehtinen, P.; Foster, A.; Pyykko, P.; Nieminen, R. Embedding Transition-Metal Atoms in Graphene: Structure, Bonding, and Magnetism. *Phys. Rev. Lett.* **2009**, *102*, 126807.
13. Dedkov, Y.; Fonin, M.; Rudiger, U.; Laubschat, C. Rashba Effect in the Graphene/Ni(111) System. *Phys. Rev. Lett.* **2008**, *100*, 107602.
14. Bogani, L.; Danieli, C.; Biavardi, E.; Bendiab, N.; Barra, A.-L.; Dalcanale, E.; Wernsdorfer, W.; Cornia, A. Single-Molecule-Magnet Carbon-Nanotube Hybrids. *Angew. Chem., Int. Ed.* **2009**, *48*, 746–750.
15. Klyatskaya, S.; Mascarós, J.; Bogani, L.; Hennrich, F.; Kappes, M.; Wernsdorfer, W.; Ruben, M. Anchoring of Rare-Earth-Based Single-Molecule Magnets on Single-Walled Carbon Nanotubes. *J. Am. Chem. Soc.* **2009**, *131*, 15143–15151.
16. Giusti, A.; Charron, G.; Mazerat, S.; Compain, J.-D.; Mialane, P.; Dolbecq, A.; Riviére, E.; Wernsdorfer, W.; Biboum, R.; Keita, B.; *et al.* Magnetic Bistability of Individual Single Molecule Magnets Grafted on Single-Wall Carbon Nanotubes. *Angew. Chem., Int. Ed.* **2009**, *48*, 4949–4952.
17. Ghirri, A.; Corradini, V.; Cervetti, C.; Candini, A.; del Pennino, U.; Timco, G.; Pritchard, R.; Muryn, C.; Winpenny, R.; Affronte, M. Deposition of Functionalized Cr_7Ni Molecular Rings on Graphite from the Liquid Phase. *Adv. Funct. Mater.* **2010**, *20*, 1552–1560.
18. Bogani, L.; Wernsdorfer, W. Molecular Spintronics Using Single-Molecule Magnets. *Nat. Mater.* **2008**, *7*, 179–186.
19. Wernsdorfer, W.; Sessoli, R. Quantum Phase Interference and Parity Effects in Magnetic Molecular Clusters. *Science* **1999**, *284*, 133–135.
20. Gatteschi, D.; Sessoli, R. Quantum Tunneling of Magnetization and Related Phenomena in Molecular Materials. *Angew. Chem., Int. Ed.* **2003**, *42*, 268–297.
21. Leuenberger, M. N.; Loss, D. Quantum Computing with Molecular Magnets. *Nature* **2001**, *410*, 789.
22. Affronte, M. Molecular Nanomagnets for Information Technologies. *J. Mater. Chem.* **2009**, *19*, 1731–1737.
23. Sanvito, S.; Rocha, A. R. Molecular-Spintronics: The Art of Driving Spin through Molecules. *J. Comput. Theor. Nanosci.* **2006**, *3*, 624–642.
24. Ferrari, A.; Meyer, J.; Scardaci, V.; Casiraghi, C.; Lazzeri, M.; Mauri, F.; Piscanec, S.; Jiang, D.; Novoselov, K.; Roth, S.; *et al.* Raman Spectrum of Graphene and Graphene Layers. *Phys. Rev. Lett.* **2006**, *97*, 187401.
25. Yan, J.; Zhang, Y.; Kim, P.; Pinczuk, A. Electric Field Effect Tuning of Electron−Phonon Coupling in Graphene. *Phys. Rev. Lett.* **2007**, *98*, 166802.
26. Arnold, D.; Bao, M.; Biang, Y.; Jiang, J.; Ma, C.; Rintoul, L.; Wang, R. Vibrational Spectroscopy of Phthalocyanine and Naphthalocyanine in Sandwich-Type (Na)Phthalocyaninato and Porphyrinato Rare Earth Complexes. *Vibr. Spectrosc.* **2004**, *34*, 283–291.
27. Fanli Lu, J. C.; Qiuhua, Y.; Yana, X. Infrared and Raman Spectroscopic Study of Tetra-Substituted Bis(phthalocyaninato) Rare Earth Complexes Peripherally Substituted with *tert*-Butyl Derivatives. *Spectrochim. Acta* **2006**, *65*, 221–228.
28. Dong, X.; Shi, Y.; Zhao, Y.; Chen, D.; Ye, J.; Yao, Y.; Gao, F.; Ni, Z.; Yu, T.; Shen, Z.; *et al.* Symmetry Breaking of Graphene Monolayers by Molecular Decoration. *Phys. Rev. Lett.* **2009**, *102*, 135501.
29. Ling, X.; Xie, L.; Fang, Y.; Xu, H.; Zhang, H.; Kong, J.; Dresselhauss, M. S.; Zhang, J.; Liu, Z. Can Graphene Be Used as a Substrate for Raman Enhancement? *Nano Lett.* **2010**, *10*, 553–561.
30. Otto, A.; Mrozek, I.; Grabhorn, H.; Akemann, W. Surface-Enhanced Raman Scattering. *J. Phys.: Condens. Mater.* **1992**, *4*, 1143.
31. Wright, A. R.; Cao, J. C.; Zhang, C. Enhanced Optical Conductivity of Bilayer Graphene Nanoribbons in the Terahertz Regime. *Phys. Rev. Lett.* **2009**, *103*, 207401.
32. Otto, A. The Chemical (Electronic) Contribution to Surface-Enhanced Raman Scattering. *J. Raman Spectrosc.* **2005**, *36*, 497–509.
33. For a concentration $C = 10^{-9}$ mol · L^{-1} and a volume of deposited drop about 1 → 10 μL, with $C = n/V \Rightarrow n =$ 10−15 mol, so 6.03×10^8 molecules. Graphene covers silicon up to 1 → 10%. So, under a laser spot of 500 nm diameter, the number of molecules on graphene is around 10 to 100 molecules.
34. Vitali, L.; Fabris, S.; Conte, A. M.; Brink, S.; Ruben, M.; Baroni, S.; Kern, K. Electronic Structure of Surface-Supported Bis(phthalocyaninato)terbium(III) Single Molecular Magnets. *Nano Lett.* **2008**, *8*, 3364–3368.
35. Gomez-Segura, J.; Diez-Perez, I.; Ishikawa, N.; Nakono, M.; Veciana, J.; Ruiz-Molina, D. Electronic Structure of Surface-Supported Bis(phthalocyaninato)terbium(III) Single Molecular Magnets. *Chem Commun.* **2006**, *27*, 2866–2868.
36. Stepanow, S.; Honolka, J.; Gambardella, P.; Vitali, L.; Abdurakhmanova, N.; Tseng, T.-C.; Rauschenbach, S.; Tait, S.; Sessi, V.; Klyatskaya, S.; *et al.* Electronic Structure of Surface Supported Bis(phthalocyaninato)terbium(III) Single

Molecular Magnets. *J. Am. Chem. Soc.* **2010**, *132*, 11900–11901.
37. Pisana, S.; Lazzeri, M.; Casiraghi, C.; Novoselov, K.; Geim, A.; Ferrari, A.; Mauri, F. Break-down of the Adiabatic Born−Oppenheimer Approximation in Graphene. *Nat. Mater.* **2007**, *6*, 198–201.
38. To estimate n, we used the formula $n = \alpha(V_g - V_{Dirac})$, where $\alpha = 7 \times 10^{10}$ cm^2/V is the value commonly accepted for a 300 nm thick SiO_2 gate dielectric and was also confirmed by Hall measurements on similar samples.
39. Novoselov, K. S.; Geim, A. K.; Morozov, S. V.; Jiang, D.; Zhang, Y.; Dubonos, S. V.; Grigorieva, I. V.; Firsov, A. A. Electric Field Effect in Atomically Thin Carbon Films. *Science* **2004**, *306*, 666–669.
40. Malard, L.; Pimenta, M.; Dresselhaus, G.; Dresselhaus, M. Raman Spectroscopy in Graphene. *Phys. Rep.* **2009**, *473*, 51–87.
41. Elemans, J.; Lei, S.; de Feyter, S. Molecular and Supramolecular Networks on Surfaces: From Two-Dimensional Crystal Engineering to Reactivity. *Angew. Chem., Int. Ed.* **2009**, *48*, 7298–7332.